International Journal of Nanomedicine

Dovepress
open access to scientific and medical research

Open Access Full Text Article

ORIGINAL RESEARCH

Ag/Au Bimetallic Nanoparticles Inhibit Tumor Growth and Prevent Metastasis in a Mouse Model

This article was published in the following Dove Press journal:
International Journal of Nanomedicine

Hector Katifelis[1]
Iuliia Mukha[2]
Penelope Bouziotis[3]
Nadiia Vityuk[2]
Charalampos Tsoukalas[3]
Andreas C Lazaris[4]
Anna Lyberopoulou[1]
George E Theodoropoulos[5]
Efstathios P Efstathopoulos[6]
Maria Gazouli[1,6]

[1]Laboratory of Biology, Medical School, National and Kapodistrian University of Athens, Athens, Greece; [2]Chuiko Institute of Surface Chemistry, National Academy of Sciences of Ukraine, Kyiv, Ukraine; [3]Radiochemical Studies Laboratory, Institute of Nuclear & Radiological Sciences & Technology, Energy & Safety, National Center for Scientific Research "Demokritos", Athens, Greece; [4]1st Department of Pathology, National and Kapodistrian University of Athens, Athens, Greece; [5]1st Propaedeutic University Surgery Clinic, Hippocratio General Hospital, Medical School, National and Kapodistrian University of Athens, Athens, Greece; [6]2nd Department of Radiology, Medical School, National and Kapodistrian University of Athens, Athens, Greece

Correspondence: Maria Gazouli
Email mgazouli@med.uoa.gr

Purpose: To evaluate the antitumor efficacy of $Ag_3Au_1Trp_{1:2}$NPs in a SCID mouse cancer model, with respect to their effect on tumor growth, on tumor's metastatic potential and the underlying molecular mechanism.

Subjects and Methods: $Ag_3Au_1Trp_{1:2}$NPs were radiolabeled with Gallium-68 and the biodistribution was studied in Swiss mice without tumors and in SCID mice bearing tumors. SCID mice received intratumoral $Ag_3Au_1Trp_{1:2}$NPs and tumor size was measured using calipers. Lung and liver tissues were extracted and studied microscopically for the detection of any metastatic sites. Changes in the Caspase-3 and TNF-related apoptosis-inducing ligand (TRAIL) were also investigated using real-time PCR and Western blot techniques, respectively.

Results: In the 4T1 tumor-bearing SCID mice, $Ag_3Au_1Trp_{1:2}$NPs showed quick passive accumulation at tumor sites at 30 mins post-injection. Mice that received the highest dose of NPs (5.6mg/mL) demonstrated a 1.9-fold lower tumor volume compared to that of the control group at 11 days post-injection, while mice that did not receive NPs showed metastatic sites in liver and lung. Extracted tumor tissue of treated mice revealed increased Casp-3 mRNA levels as well as elevated TRAIL protein levels.

Conclusion: Based on our results, $Ag_3Au_1Trp_{1:2}$NPs express anti-tumor and anti-metastatic effects in vivo. $Ag_3Au_1Trp_{1:2}$NPs also reach tumor site via the enhancement and retention effect which results in the apoptotic death of cancerous cells selectively via the extrinsic TRAIL-dependent pathway.

Keywords: nanoparticles, cancer, SCID mice, TRAIL, Casp-3

Introduction

The rapid advances in nanomedicine have recently generated an increasing number of promising cancer diagnostic and therapeutic applications.[1–3] Among the different types of nanoparticles, chemically synthesized metal nanoparticles have well-known use across the biomedical sciences as novel therapeutic agents, especially gold and silver nanoparticles (Au/Ag NPs) with several studies confirming their anti-tumor efficiency in vitro and in vivo.[4–6] In vivo applications of nanoparticles face several challenges including the formation of the "biomolecular corona", which may accelerate clearance from the bloodstream[7] and increased liver uptake, which could lead to toxicity.[8] Additionally, the intensity of the enhanced and retention permeability effect (EPR effect), which allows passive targeting of tumor tissues due to malformed blood vessels and poor lymphatic drainage, remains difficult to predict.[8] Our previous studies[3,9] showed that bimetallic Ag/Au NPs synthesized as "alloy" via a chemical reduction method using Tryptophan (TRP)

with a metal ratio of 3:1 and double molar excess of TRP [Ag/Au NPs ν(M):ν(Trp) = 1:2], had the maximal anti-cancer effect. In the present study, $Ag_3Au_1Trp_{1:2}$NPs were tested regarding their anti-cancer activity in a SCID mouse cancer model, using the highly metastatic mouse breast cancer cell line 4T1. In vivo studies included the administration of ^{68}Ga-NOTA-DMSA $Ag_3Au_1Trp_{1:2}$NPs in SCID mice, to reveal their uptake in cancer tissues. $Ag_3Au_1Trp_{1:2}$NPs were also administered in a group of tumor-bearing mice, in order to determine tumor growth in direct comparison to a control group which was injected with saline. At the same time ex vivo, studies were performed to measure the therapeutic efficacy of $Ag_3Au_1Trp_{1:2}$NPs in primary tumor tissue via histopathology. In order to clarify more aspects regarding the effect of $Ag_3Au_1Trp_{1:2}$NPs on metastatic potential, we conducted the in vitro wound closure assay to test alterations in the migratory processes of cancer cells. Furthermore, ex vivo histopathology showed the topology of $Ag_3Au_1Trp_{1:2}$NPs in cancer tissues, as well as their effect on metastasis formation (in lung and liver tissue). Further to our previous study, supporting that $Ag_3Au_1Trp_{1:2}$NPs exhibit their anti-cancer properties in vitro by inducing the P53, Caspase-3 (Casp-3), bax/bcl-2 apoptotic pathways, in this study we tested the expression of cancer-related TNF-Related Apoptosis-Inducing Ligand (TRAIL) and the subsequent expression of Casp-3 in SCID mice cancer tissues, aiming at increasing our knowledge on the biological activity of $Ag_3Au_1Trp_{1:2}$NPs.

Materials and Methods

Nanoparticle Synthesis

Colloidal solutions of monometallic and bimetallic silver and gold NPs were obtained via chemical reduction of silver nitrate ($AgNO_3$) and tetra-chloroauric acid ($HAuCl_4$) with amino-acid tryptophan as already described.[3] The metal concentration in final solutions was C(M) = 10^{-4} mol/L, while the molar ratio of components for all colloids was ν(M):ν(Trp) = 1:2. For all colloids, the initial solutions of Trp were adjusted to pH = 10 with 1 N NaOH and heated to boiling, followed by injection of $AgNO_3$/$HAuCl_4$ solutions.

Cell Culture & Wound Closure Study

In order to investigate if Ag/Au NPs affect the metastatic potential of 4T1 cells, we performed a wound closure assay protocol.[10] 4T1 cells (mouse-derived malignant breast tumor of high metastatic potential) purchased from American Type Culture Collection (ATCC® CRL-2539™ Rockville, MD) were grown in DMEM High Glucose culture medium (BioSera) containing 10% FBS, 2mmol/L glutamine, 100U/mL penicillin and 100g/mL streptomycin at 37°C. When cells reached 70% confluence, they were placed in 6-well plates. Briefly, when cells reached a nearly 100% confluence a vertical wound was made, using a sterile tip. Then, the following NPs were tested: $Ag_3Au_1Trp_{2:1}$NPs NPs (in three concentrations, 30, 40 and 50μg/mL), $AgTrp_{1:2}$NPs (40μg/mL) and $AuTrp_{1:2}$NPs (40μg/mL) to investigate their effect upon wound closure. A negative control was also used (cells that received no treatment). Photographs were taken at 0, 3, 6, 9, 12 and 24hrs observing the wound closure process. The protocol was completed after 24hrs when untreated cells had a full wound closure. All experiments were held in duplicate.

Gallium-68 Radioactivity

Radioactivity of the Gallium-68 eluent was measured using a dose calibrator (Capintec, Ramsey, NJ). Thin-layer chromatography (TLC) silica gel 60 sheets (5 × 10 cm) were purchased from Merck (Darmstadt, Germany) and along with a Radio-TLC Scanner (Scan-Ram, LabLogic, Sheffield, UK) were used in the determination of radiolabeling yield/purity. Amicon filters (molecular weight cut-off value: 100 kD) were used for purification of the functionalized nanoparticles. Water was deionized to 18 M·cm using an easy-pure water filtration system (Barnstead International, Dubuque, Iowa). A lower activity commercial ^{68}Ge/^{68}Ga generator was acquired from ITG Garching (Garching, Germany). 30% HCl Suprapur (Merck, Darmstadt, Germany), acetone and ammonium acetate (Sigma-Aldrich) were used as received. A gamma scintillation counter, a Packard Cobra II (Canberra, Packard, Downers Grove, IL, USA), was used to measure the radioactivity of each organ and blood samples in the ex vivo biodistribution studies.

Functionalization of NPs with Mal-NOTA-MPAA

All nanoparticles samples (AgAu ratio 1:1, AgAu 3:1, Ag and Au) were incubated with 0.027 mmol DMSA dissolved in 1mL DMSO and left overnight on a stirring apparatus at RT. The functionalized NPs were purified by centrifugation using Amicon filters (MWCO 100 kD, 10,000 rpm, 10mins). The nanoparticles were washed

twice with 500 μL ultrapure H_2O by centrifugation and were redispersed in 100 μL DMSO. Then, 200 μg of the chelator mal-NOTA-MPAA (Chematech, France) dissolved in DMSO were added to the DMSA-functionalized NPs, and were stirred overnight at RT. The resulting NOTA-DMSA-NPs were purified as described above, reconstituted with ultrapure water and were further used for radiolabeling with Gallium-68.

Radiolabeling of Nanoparticles with Gallium-68

For the radiolabeling experiment, ^{68}Ga was eluted from the ^{68}Ge/^{68}Ga generator, using freshly prepared, trace-free solvents.[11] A fraction containing $^{68}GaCl_3$ (~25MBq) in a volume of 100 μL was used. Radiolabeling was performed by mixing 50 μL of each NP suspension, 350 μL of sodium acetate buffer (0.2M, pH 4), and 100 μL of $^{68}GaCl_3$ and incubating at 70°C for 30 min. The radiolabeling yield was determined by thin-layer chromatography analysis (TLC). The strip was developed using citric acid 0.1M as the mobile phase. With this system, ^{68}Ga-NOTA-DMSA-NPs remained at the application point, while unbound $^{68}Ga^{3+}$ ions migrate with the solvent front.

Biodistribution Studies

Animals used for the biodistribution studies were obtained from the breeding facilities of the Institute of Biosciences and Applications, NCSR "Demokritos". Our experimental animal facility is registered according to the Greek Presidential Decree 56/2013 (Reg. Number: EL 25 BIO 022), in accordance to the European Directive 2010/63 which is harmonized with national legislation, on the protection of animals used for scientific purposes. All applicable national guidelines for the care and use of animals were followed. The study protocol was approved by the Department of Agriculture and Veterinary Service of the Prefecture of Athens (Protocol Number: 1607/11-04-2018). The animals were housed in air-conditioned rooms under a 12 h light/dark cycle and allowed free access to food and water.

Initial studies of all 4 chelator-functionalized NP samples were performed on normal Swiss mice, to assess their in vivo behavior (n = 4 mice, animal weight 22–25 g). Each radiolabeled NP sample was intravenously administered via the tail vein (100 μL, ~1 MBq).

For further assessment of the functionalized NPs in tumor-bearing SCID mice, the $Ag_3Au_1Trp_{1:2}$NPs were selected, as they demonstrated the largest toxicity gap in cancerous and non-cancerous cells, as shown in our previous cell studies.[3] For the development of experimental tumor models, female SCID mice of 8 weeks on the day of inoculation were subcutaneously inoculated with 4T1 cells (1×10^7 cells). Approximately 7 days after inoculation, ex vivo biodistribution studies were performed on the tumor-bearing mice. ^{68}Ga-NOTA-DMSA- Ag3Au1Trp1:2NPs were administered via the tail vein (n = 4 mice, animal weight 18–20 g). Each mouse received 100 μL (~1 MBq) of the radiolabeled NP.

For both ex vivo biodistribution experiments described above, the animals were euthanized at 30, 60, and 120 mins post-injection, and the organs of interest (liver, heart, kidneys, stomach, intestines, spleen, muscle, lung, bone, pancreas) as well as the tumor (in the case of the tumor model), were removed, weighed and counted in a NaI well-counter. The remaining radioactivity in the tail, as well as background counts, were subtracted and the radioactivity decay was auto-corrected by the counter. The uptake of the radiolabeled NPs in each organ was expressed as the percentage injected dose per gram of tissue (%IA/gr ± SD) and calculated compared to the activity of a standard dose of the injected solution.

Therapeutic Efficacy Studies

The effect of $Ag_3Au_1Trp_{1:2}$ nanoparticles on tumor growth was determined in SCID mice bearing subcutaneous 4T1 breast cancer xenografts when the tumor reached volume of about 300 mm^3 (about 7 d after cell inoculation). Mice were randomly divided into 2 groups (n = 4 mice per group) and received three intratumoral injections of either normal saline (control group, 100 μL saline) or $Ag_3Au_1Trp_{1:2}$NPs (therapy group, 100 μL NPs) (days of injection designated as Day 1, Day 3 and Day 5). Tumor volume was monitored for 12 days using calipers and was calculated using the formula (length × $width^2$)/2.[12,13] Tumor growth was plotted vs treatment time post-injection.

Histopathology Study

Upon euthanasia, tumor, lung and liver tissue were surgically extracted from every mouse and fixed in 10% formalin, embedded in paraffin and sectioned. Then, the slides were stained with Hematoxylin and Eosin stain (H&E) and studied on a light microscope (Olympus CX-31, Melville, NY, USA, with ToupView image analysis software, ProWay/ToupTek Protonic, Hangzhou, China).

Nanoparticle Visualization

The sections used in the histopathology studies were also used to confirm the presence of NPs in the cancer tissue; sections without H&E were used. NP visualization was performed using Silver Enhancer Kit (Light Insensitive, abcam, ab17033) according to the manufacturer's instructions. Methylene blue was used as a counter stain.

RNA Extraction, cDNA Synthesis and Casp-3 Expression Analysis

Total RNA was extracted from cancer tissues obtained from SCID mice with and without treatment, using Nucleozol (Macherey-Nagel). cDNA synthesis was performed using the PrimeScript First-strand cDNA synthesis kit (TAKARA). One microgram RNA was incubated for 30mins at 37°C followed by 85°C for 5s in a reaction containing 500μg of Oligo dT, 10mM deoxyribonucleotide triphosphates 5X first-strand buffer 0.1M dithiothreitol and 200U/mL reverse transcriptase. The reaction was held on a Thermal cycler (Kyratec Super Cycler). mRNA levels of *Casp-3* were studied using *GAPDH* expression levels as a reference gene. Quantitive real-time PCR was performed on an ABI Prism apparatus (Applied Biosystems, Foster City, CA, USA) by mixing cDNA samples with Casp-3 a set of primers (Forward: 5′- TGGTTCATCCAGTCGCT TTG −3′, Reverse: 5′-CATTCTGTTGCCACCTTTCG-3′) and PCR master mix (KAPA SYBR FAST qPCR Kit). Gene expression levels were normalized by subtracting Ct value of the *GAPDH* RNA from that of Casp-3 using the equation ($\Delta Ct = -|Ct_{GOI} - Ct_{GAPDH}|$). Relative expression of Casp-3 was determined comparing the samples from mice that received treatment with those who did not, using the $2^{\Delta\Delta Ct}$ model in which $\Delta\Delta Ct = \Delta Ct_{GOI} - \Delta Ct_{GAPDH}$. Casp-3 expression was calculated using the FAST qPCR Kit for real-time PCR. mRNA levels were quantified using SYBR Green dye and all samples were held in duplicate.

Western Blotting

Proteins from cancer tissue (4T1 cells) removed from SCID mice were extracted (mice with and without treatment). For this process, a lysis buffer containing protease inhibitors and the mechanical homogenization were used. Protein concentration was quantified using the Bradford method. All samples were loaded into a 10% polyacrylamide gel with equal amount of proteins (30μg per sample) and they were electrotransferred. Fat-free milk was used for blocking of non-specific binding sites. The membrane was incubated with the primary antibody (TRAIL H-257, sc-7877, Santa Cruz Biotechnology Inc) at 4°C for 12–16hrs. After a 1hr incubation with the secondary antibody (goat anti-rabbit, Millipore AP132P) the formed complexes were visualized using chemiluminescence (Pierce ECL Western Blot Substrate). Protein expression was normalized using b-actin (mab1501, Millipore and goat-anti rabbit, Millipore AP132P as the secondary antibody). Molecular weights for TRAIL and b-actin are 34 and 47kDa, respectively.

Statistical Analysis

All statistical analyses were performed using GraphPad version 3.00 (GraphPad Software, San Diego, CA). $p>0.05$ was considered significant.

Results

In order to test the anti-cancer effect of $Ag_3Au_1Trp_{1:2}$NPs we performed further in vitro and in vivo studies:

1. We tested in vitro the effect of $Ag_3Au_1Trp_{1:2}$NPs in cell migration, a process involved in several pathological processes such as tumor invasion, neoangiogenesis and metastasis. In order to achieve this, we performed a Wound closure assay of 4T1 cells.
2. In vivo studies included the administration of ^{68}Ga-NOTA-DMSA $Ag_3Au_1Trp_{1:2}$NPs in SCID mice, to reveal their biodistribution and therapeutic effect in cancer tissues.
3. Ex vivo studies were performed to measure the therapeutic efficacy of $Ag_3Au_1Trp_{1:2}$NPs in tumor tissue via histopathology.

$Ag_3Au_1Trp_{1:2}$NPs Attenuate the Migratory Potential of 4T1

In order to test the effect of $Ag_3Au_1Trp_{1:2}$NPs in cancer metastasis, we performed in vitro the wound healing assay, since cell migration and invasion are key processes in cancer metastasis that offer many opportunities for therapeutic intervention. A "wound" was introduced in 4T1 confluent plates that gave us the opportunity to follow cell movement and morphology for 24 hrs under the conditions of the experiment. Wound closure percentage was calculated by using the following formula: 100% – wound length at each time point/wound length

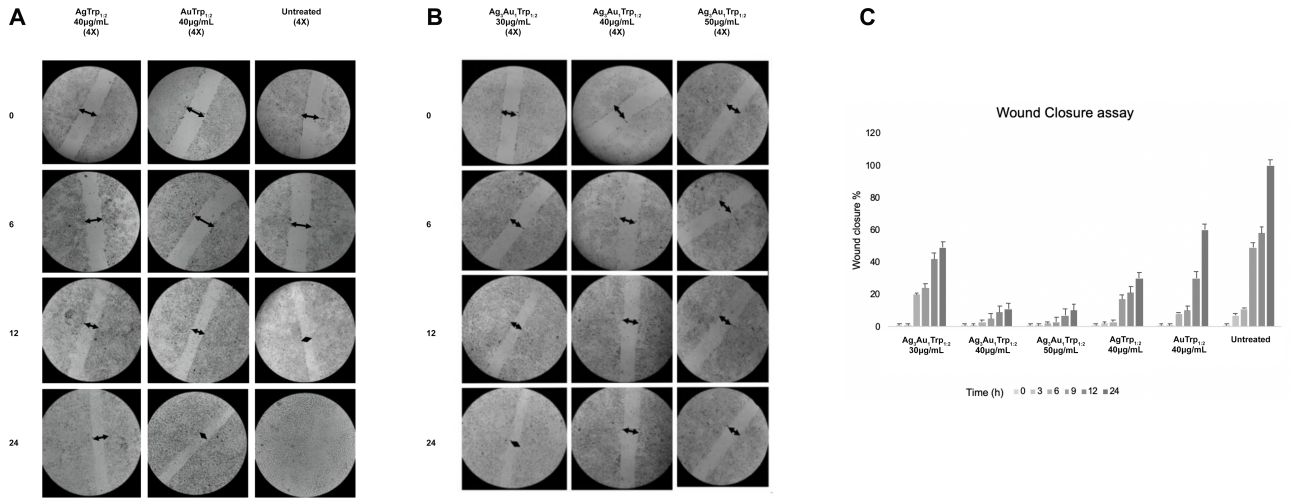

Figure 1 (**A**) Wound closure assay of 4T1 cells incubated with $Ag_3Au_1Trp_{1:2}$NPs (30, 40 and 50μg/mL). (**B**) Wound closure assay of 4T1 cells incubated with AgNPs (40μg/mL), AuNPs (40μg/mL) and untreated cells. Photographs were taken at several time points to observe the closure process. (**C**) Wound closure percentages at various time points (0, 3, 6, 9, 12 and 24 hrs) at 4T1 cells incubated with $Ag_3Au_1Trp_{1:2}$NPs (30, 40 and 50μg/mL) NPs, AgNPs (40μg/mL) and AuNPs (40μg/mL). Cells that received no treatment were used as control. All experiments were held in duplicate.

at time point zero. Wound length was estimated as the length of the wound (cell-free-layer, indicated by the arrows in Figure 1A and B) in mm. Monometallic Ag and Au NPs, as well as untreated cells were used as control plates (Figure 1A). We observed that in the untreated cell plates the cell-free zone is closed after 24 hrs via the metastatic potential of 4T1 cells. The case is not the same under the effect of monometallic Ag and Au NPs: the migration of 4T1 cells was not enough to fill the void during the same time period (24 hrs) (Figure 1A). In detail, we noticed that cell migration in untreated cells managed to cover the void at 7% in the first 3 hrs and reached almost 60% in 12 hrs. At the end, there was no cell-free zone observed after 24 hrs. At the same time, under the effect of Ag and Au NPs, the cell-free zone was covered $Ag_3Au_1Trp_{1:2}$NPs at 3% and 8% in 6 hrs and 30% and 60% in 24 hrs respectively (Figure 1C). Regarding the $Ag_3Au_1Trp_{1:2}$NPs, we interestingly showed an obstruction of the migratory potential of tumor cells, since the cell-free zone as we notice in Figure 1B is slightly closed for the 40 μg/mL and 50 μg/mL NP concentrations. Namely, the void was only covered at approximately 10% after 24 hrs under the effect of 40 μg/mL $Ag_3Au_1Trp_{1:2}$NPs. Almost the same effect was observed with the 50 μg/mL concentration, while the effect of 30 μg/mL $Ag_3Au_1Trp_{1:2}$NPs in the migratory potential of 4T1 cells was shown to be milder with 20% of cell-free zone coverage after 6 hrs and almost 50% after 24 hrs (Figure 1C).

Radiolabeling of $Ag_3Au_1Trp_{1:2}$NPs and in vitro Stability Assessment

In order to examine the biodistribution of $Ag_3Au_1Trp_{1:2}$ NPs, we proceeded to radiolabel them with the positron emitter ^{68}Ga. ^{68}Ga-NOTA-DMSA- $Ag_3Au_1Trp_{1:2}$NPs were radiolabeled after 30 min incubation at 70°C. Radiochemical yield was assessed by ITLC and was found to be ~90 ± 1.5%. The radiolabeled NPs were subjected to purification by centrifugation with ultracentrifugation filters. ITLC assessment demonstrated a radiochemical purity of > 93% for the radiolabeled NPs. The sample was diluted with water for injection for biodistribution experiments.

In order to assess the in vitro stability of ^{68}Ga-NOTA-DMSA- $Ag_3Au_1Trp_{1:2}$NPs in various solutions, the radiolabeled sample was incubated with PBS for 120 min at RT, and was found to be practically stable (>98% retention of the radiolabel). In order to assess in vivo stability of the radiotracer under development, serum stability testing is performed. These results demonstrated satisfactory in vitro stability in the presence of serum, up to 120 mins post-incubation (>92% retention of the radiolabel), as evaluated by ITLC analysis. Further assessment was not possible, due to the short half-life of ^{68}Ga.

$Ag_3Au_1Trp_{1:2}$NPs Biodistribution in RES and Tumor Sites

Biodistribution studies were performed on healthy Swiss mice (for all 4 NP structures) and on 4T1 tumor-bearing

SCID mice (for $Ag_3Au_1Trp_{1:2}$NPs), after their radiolabeling with ^{68}Ga, in order to provide information on their in vivo kinetics. All radiolabeled NPs were administered via the tail vein. The accumulation of ^{68}Ga-NPs in the organs at 30, 60- and 120-min post-injection is shown in Figure 2 (Panels A, B, C and D), as percentage of injected dose per gram of tissue (% ID/g ± SD). All four NP species demonstrated fast blood clearance, with <2% ID/g remaining in the bloodstream at 2hrs p.i. After organ distribution through blood, high levels of radioactivity were observed for all NPs in the lung, liver and spleen, organs of the Reticuloendothelial System (RES). In the 4T1 tumor-bearing SCID mice, the ^{68}Ga-NOTA-DMSA- $Ag_3Au_1Trp_{1:2}$NPs demonstrated quick passive accumulation in the tumor, starting at 2.26 ± 0.47% ID/g at 30 min p.i., slightly decreasing at 60 min p.i. (1.48 ± 0.09% ID/g) and then increasing at 120 mins p.i. (1.75 ± 0.46% ID/g). Tumor-to-muscle ratios demonstrated an upward trend, from ~2.5 at 30 mins to ~4 at 120 mins.

Effect of $Ag_3Au_1Trp_{1:2}$NPs on Tumor Growth

The therapeutic efficacy of $Ag_3Au_1Trp_{1:2}$NPs was determined by estimation of the Tumor Volume of four groups of 4T1 tumor-bearing SCID mice, up to 11 days post-treatment by intratumoral injection of $Ag_3Au_1Trp_{1:2}$NPs (Therapy Group A: 0.4 mg/mL; Therapy Group B: 4.0 mg/mL, Therapy Group C: 5.6 mg/mL) and normal saline (Control Group). Mice in Groups A, B and C received three injections of $Ag_3Au_1Trp_{1:2}$NPs, while mice in the Control Group received three injections of normal saline, on Day 1 (day of treatment initiation), Day 3 and Day 5. Tumor volume of Therapy Group C mice was ~1.7-fold lower than the Control Group mice at 8 days p.i. and showed an increasing trend, reaching ~1.9-fold lower at 11 days p.i. (Figure 3A–C).

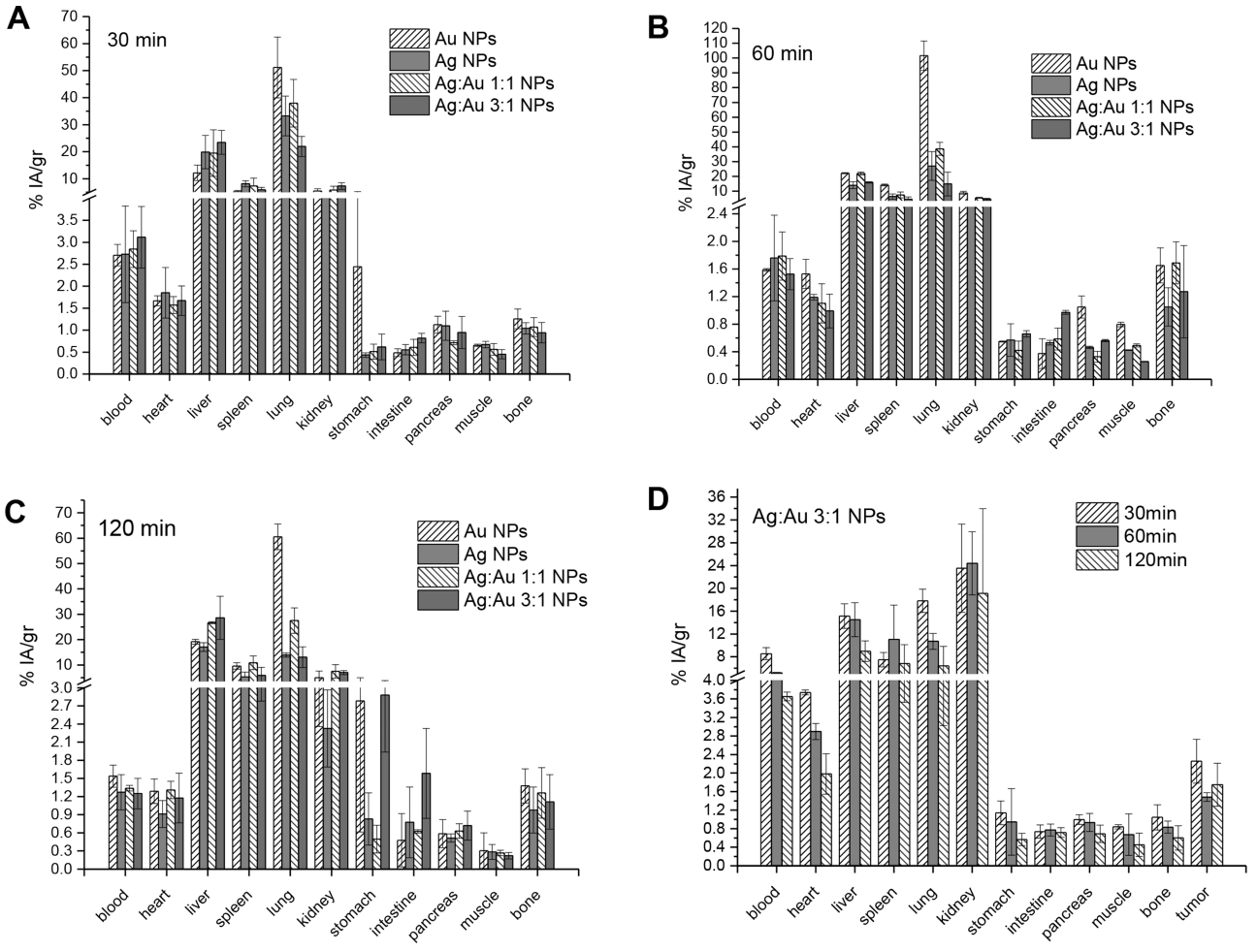

Figure 2 Ex vivo biodistribution studies of ^{68}Ga-labeled NPs. (**A**–**C**) Evaluation in normal Swiss mice at 30, 60 and 120 mins p.i.; (**D**) Evaluation of ^{68}Ga-NOTA-DMSA- $Ag_3Au_1Trp_{1:2}$NPs in 4T1 tumor-bearing SCID mice at 30, 60 and 120 mins p.i.

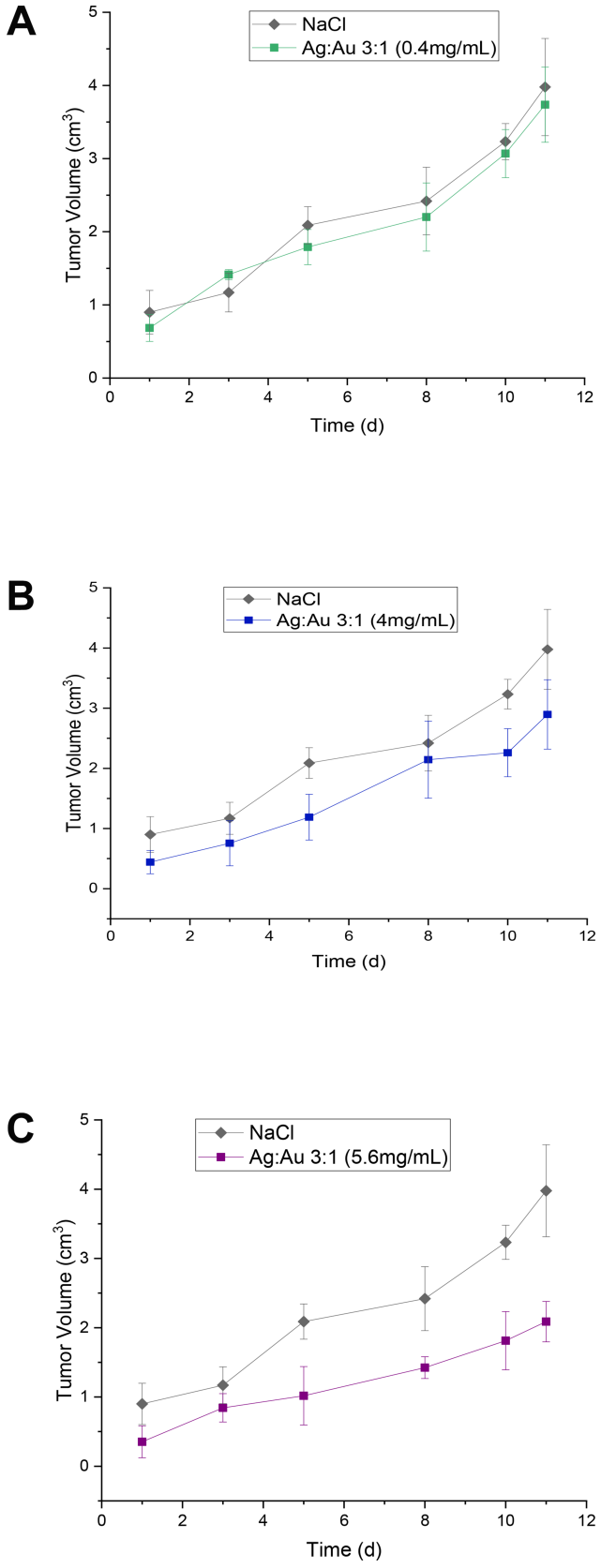

Figure 3 Effect of intratumoral injection of $Ag_3Au_1Trp_{1:2}$NPs (three different concentrations) or normal saline on the Tumor Volume of 4T1 tumor-bearing SCID mice. Values represent the mean ± SD (n = 3 mice per group). (**A**–**C**) show the difference in tumor volume of each concentration of $Ag_3Au_1Trp_{1:2}$NPs in direct comparison to the Control Group (untreated).

Table 1 Metastatic Sites in Liver and Lung of SCID Mice That Received $Ag_3Au_1Trp_{1:2}$NPs Treatment (Mice 1, 2, 3) and SCID Mice from the Respective Control Group (Mice 4, 5, 6)

SCID Mouse	Treatment	Dose	Liver Metastasis	Lung Metastasis
1	Yes	5.6mg/mL	No	No
2	Yes	5.6mg/mL	No	No
3	Yes	5.6mg/mL	No	No
4	No	–	No	Yes
5	No	–	No	Yes
6	No	–	Yes	Yes

$Ag_3Au_1Trp_{1:2}$NPs Accumulate in Cancer Tissues and Block Metastasis

Table 1 shows the metastatic sites found on SCID mice that received 5.6 mg/mL intratumoral injection and their respective control group. Tumor tissues are shown in Figure 4 (Figure 4A and B show tumor tissue from mice that received treatment and Figure 4C and D show tumor tissue from mice that did not). None of the mice that received treatment showed metastatic sites neither in the lungs nor in the liver (Figure 5A and B, 6A-B, respectively). Figure 6C shows liver tissue from a mouse that did not receive treatment and did not show any metastatic sites. On the contrary, metastatic sites are present in the lungs (Figure 5C–F) and in the liver (Figure 6D) of mice that did not receive treatment. $Ag_3Au_1Trp_{1:2}$NPs are visualized in tumor tissue sections; white arrows indicate dark dots that are formed around NPs, as shown in Figure 7A and C. Background staining was minimal. Figure 7B and D indicate controls without $Ag_3Au_1Trp_{1:2}$NPs treatment.

TRAIL Over-Expression After $Ag_3Au_1Trp_{1:2}$NPs Treatment

TRAIL is a cytokine that is produced and secreted by most normal tissue cells. It causes apoptosis primarily in tumor cells, by binding to certain death receptors. Herein, we found that TRAIL is significantly over-expressed in cancer tissues under $Ag_3Au_1Trp_{1:2}$NPs treatment ($p = 0.023$) as seen in the Western blot results (Figure 8).

$Ag_3Au_1Trp_{1:2}$NPs Up-Regulated Caspase-3 Expression

Several molecular mechanisms can result in the up-regulation of Casp-3 including T-cell receptor activation and ligation of FasL and TRAIL with their respective receptors.[14,15] Thus, we tested if the over-expression of TRAIL in mice that received $Ag_3Au_1Trp_{1:2}$NPs would also lead to the downstream Casp-3 up-regulation and the cleavage of the death substrates. Levels of *Casp-3* mRNA (in tumor tissue from mice that received $Ag_3Au_1Trp_{1:2}$NPs treatment) were quantified via real-time PCR and were found up-regulated by 4.59 times compared to mice that received no treatment (Figure 9).

Discussion

Bimetallic nanoparticles (BNPs) are constructed via the combination of two different metals, with each metal offering different properties. BNPs show novel electronic, optical and catalytic or photocatalytic properties due to synergistic effects, and thus they act in a different way in biological systems when compared with MNPs. Because of their unique properties and their superiority over monometallic nanoparticles (MNPs), BNPs are proposed as promising tools for therapy and diagnosis. However, most of the studies are evaluating their use in cancer imaging and diagnostic applications, rather than their therapeutic potential. Recently, Shmarakov et al reported that Ag/Au NPs inhibit mouse Lewis lung carcinoma (LLC) growth in vivo suggesting that the observed antitumor activity of the studied NPs strongly depends on Ag/Au interaction arising from their ordered topological distribution.[6]

In support of this, we present the antitumor effect of $Ag_3Au_1Trp_{1:2}$NPs in SCID mice. Ag and Au are often used in bimetallic constructions due to the ease in synthesis. Furthermore, Ag NPs are known to show anticancer and antibacterial effects via ROS generation and subsequent apoptotic mechanisms, while AuNPs are famous in vivo NPs due to their minimum toxicity and thus their ease in entering the cells via EPR effect. In our previous study,[9] we showed that $Ag_3Au_1Trp_{1:2}$NPs demonstrated an antitumor effect in vitro in cancer cell lines. Most importantly, the toxicity was remarkably higher in cancer cell lines, compared to non-cancerous cell lines, an effect not obvious with MNPs, providing to BNPs a specialty in cancer cells without the use of a target moiety. So, in the present study, we wanted to check the same effect in vivo and whether BNPs could be used as antitumor and anti-metastatic therapeutic drugs. Initially, we conducted biodistribution studies in order to extract information regarding their in vivo kinetics. After intravenous injection, the NPs enter the blood circulation to end up in blood flow organs and peripheral tissues, while their biodistribution in tissue mainly depends on their size and surface charge. Fast blood clearance in our study

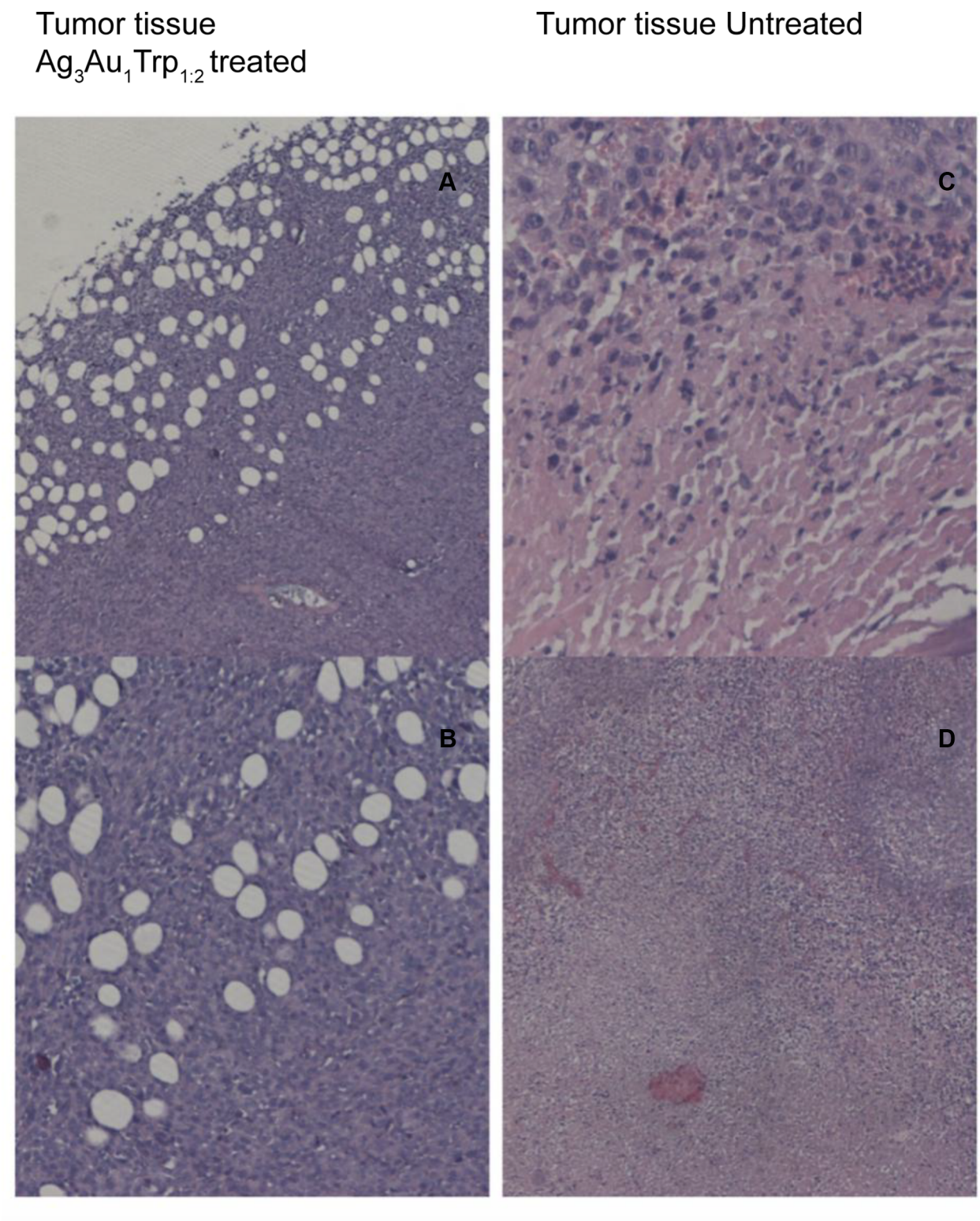

Figure 4 Tumor histological study. Fat tissue infiltration by low differentiated cancer cells with atractoid morphology (**A** and **B** mice that received $Ag_3Au_1Trp_{1:2}$NPs). (**C** and **D**) show tumor tissue with low differentiation with necrotic sites and acute inflammation from mice that received no treatment.

may be attributed to the rapid accumulation of these NPs in the lungs and liver. All 4 NP species are cleared mostly through the hepatobiliary system, since their diameter is larger than the 5nm size, which justifies renal clearance.[16,17] Nonetheless, there is an estimable kidney uptake, which can be attributed to partial clearance of the

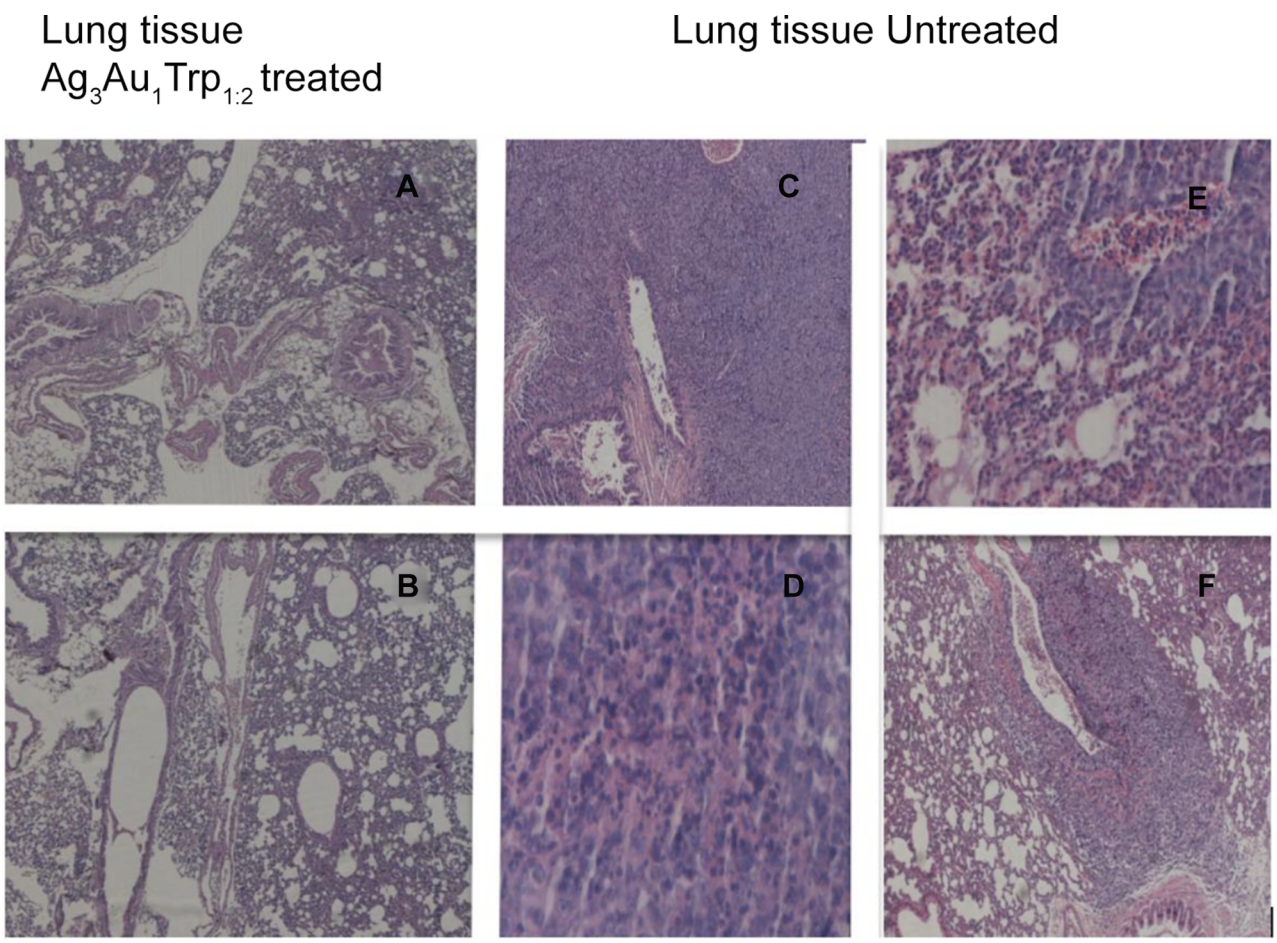

Figure 5 No metastatic sites were found in mice that received $Ag_3Au_1Trp_{1:2}$NPs (**A** and **B**). Mice that did not receive treatment showed several metastatic sites (**C**–**F**).

NPs through the kidneys. Lung uptake was high for all NP species at all three time-points but was significantly higher for the ^{68}Ga-NOTA-DMSA-Au NPs (60.53 ± 5.08% ID/g at 120 mins p.i.). The pronounced lung uptake may be attributed to various factors, such as NP size and DMSA coating.[18–20] Most importantly, almost 2.5% ID/g of $Ag_3Au_1Trp_{1:2}$NPs accumulated to the tumor sites at 30 min post-administration (Figure 2D). Generally, the ideal NP has to stay enough time to bloodstream in order to augment the possibility to reach the tissue of interest, after escaping the RES which is one of the major biological barriers that reduce NP accumulation to the target tissue. Once reaching the target tissue, NPs are faced with endothelial and cellular obstacles.[21] With regard to the 4T1 tumor-bearing group of SCID mice, almost 2.3% ID/g of $Ag_3Au_1Trp_{1:2}$NPs accumulated to the tumor sites at 30 min post-administration (Figure 2D). $Ag_3Au_1Trp_{1:2}$NPs were passively targeted to the tumor tissue, namely NPs accumulated to the target tissue via the EPR effect. Taking into consideration that only a median of 1% approximately of the total-administered NP dose is usually able to reach a solid tumor, the percentage of ~2.3% ID/g of $Ag_3Au_1Trp_{1:2}$NPs at 30mins is quite high.[22] Tumor-to-muscle ratios increased from ~2.7 at 30 min p.i. to ~4 at 120 mins p.i., thus showing efficient clearance of the radiotracer from the rest of the body. Histopathological studies also revealed the accumulation of $Ag_3Au_1Trp_{1:2}$NPs to the tumor tissue (Figure 7).

Subsequently, we injected $Ag_3Au_1Trp_{1:2}$NPs intratumorally in SCID mice bearing 4T1 tumors and monitored tumor growth over a period of 11 days, in order to evaluate their therapeutic effect in the primary tumor. The group of mice injected with the highest NPs concentration (5.6 mg/mL) showed the highest tumor growth retardation after 11 days, when compared to the control group of mice, which were injected with saline (tumor volume ~1.9-fold lower for the therapy group, in direct comparison to the control group of mice). Therefore, we can assume that $Ag_3Au_1Trp_{1:2}$NPs show in vivo antitumor effect in tumor-bearing SCID mice. In addition, we also wanted to test whether $Ag_3Au_1Trp_{1:2}$NPs could reduce the metastatic process

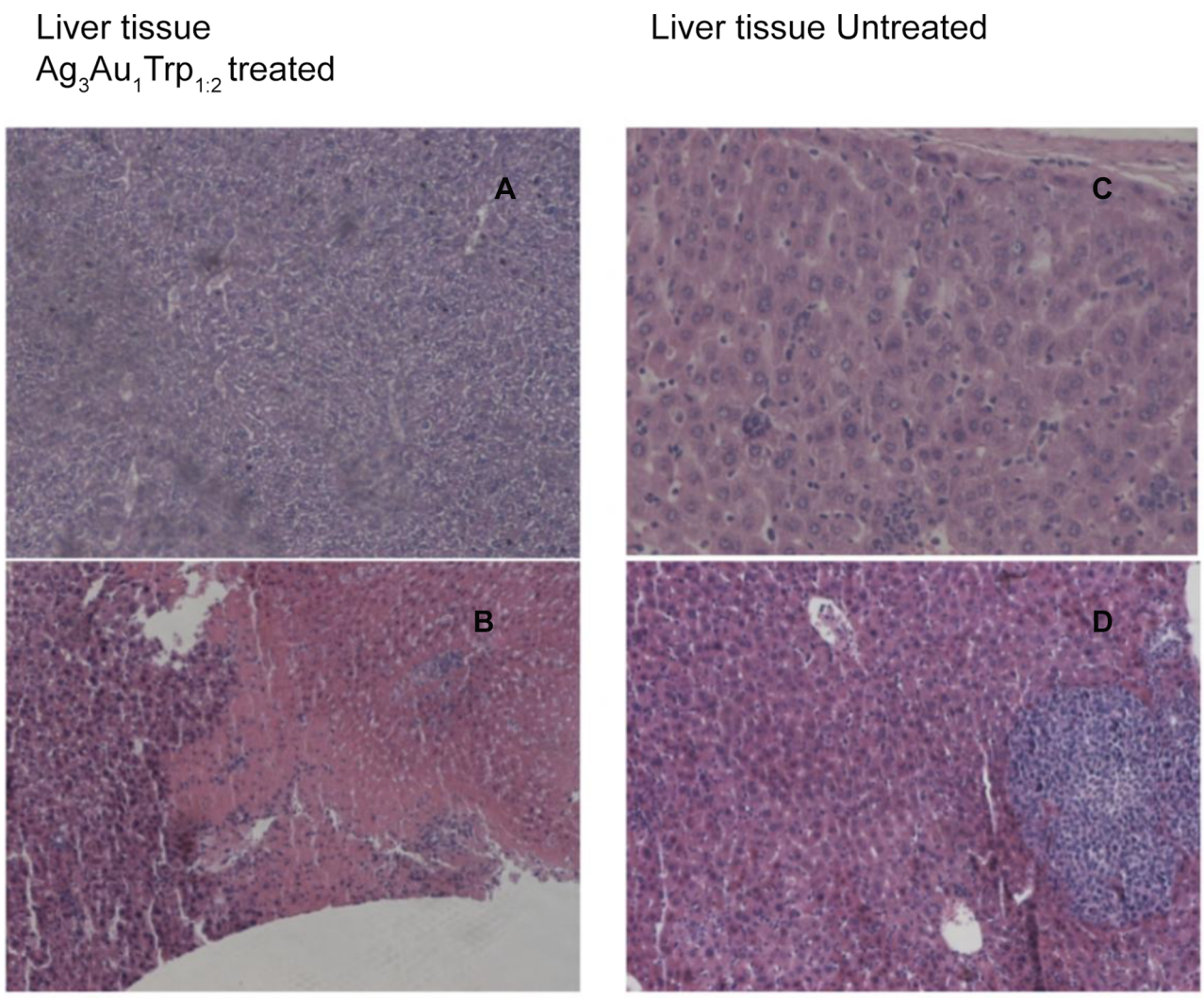

Figure 6 Liver histology study of mice that received (**A** and **B**) and mice that did not receive (**C** and **D**) treatment. All mice (treated with $Ag_3Au_1Trp_{1:2}$NPs and untreated) showed inflammation and metastatic sites were observed in one liver tissue of a mouse that did not receive treatment (**D**).

in vitro conducting the wound closure assay and ex vivo via histopathological studies of the metastatic sites of SCID mice. Indeed, treating 4T1 cells with $Ag_3Au_1Trp_{1:2}$ NPs (concentrations 40 and 50μg/mL) inhibited the wound closure process; only a tenth of the healing process was completed at the time point that untreated 4T1 cells showed full wound closure (Figure 1B and C). This anti-metastatic effect was also observed in vivo; mice that received $Ag_3Au_1Trp_{1:2}$NPs showed no metastatic sites in either the lungs or the liver (Table 1).

In a previous study,[3] we found that BNPs induce apoptosis in vitro via P53, Casp-3 and Bax/Bcl-2 pathway. Therefore, the anticancer effect of $Ag_3Au_1Trp_{1:2}$NPs could partially be explained by the fact that they trigger apoptotic responses in cancer cells, through the generation of ROS that causes oxidative stress and subsequent DNA damage. However, besides the intrinsic apoptotic pathway, we thought that there must also be an extrinsic pathway explaining the anti-tumor and anti-metastatic effect of $Ag_3Au_1Trp_{1:2}$NPs, as well as the specificity of this effect in cancer cells comparing to non-cancerous cells. TRAIL-induced apoptosis shows selectivity towards cancer cells, but, on the other hand, does not induce apoptosis in most normal cells. TRAIL is a ligand included in the TNF (Tumor Necrosis Factor) (TNF) family of ligands capable of initiating apoptosis through their conjugation with its death receptors.[23] Targeting death and decoy receptors of the tumour-necrosis factor superfamily. . Trimerization of the latter and their death domains (DDs), respectively, leads to the formation of the death-inducing signaling

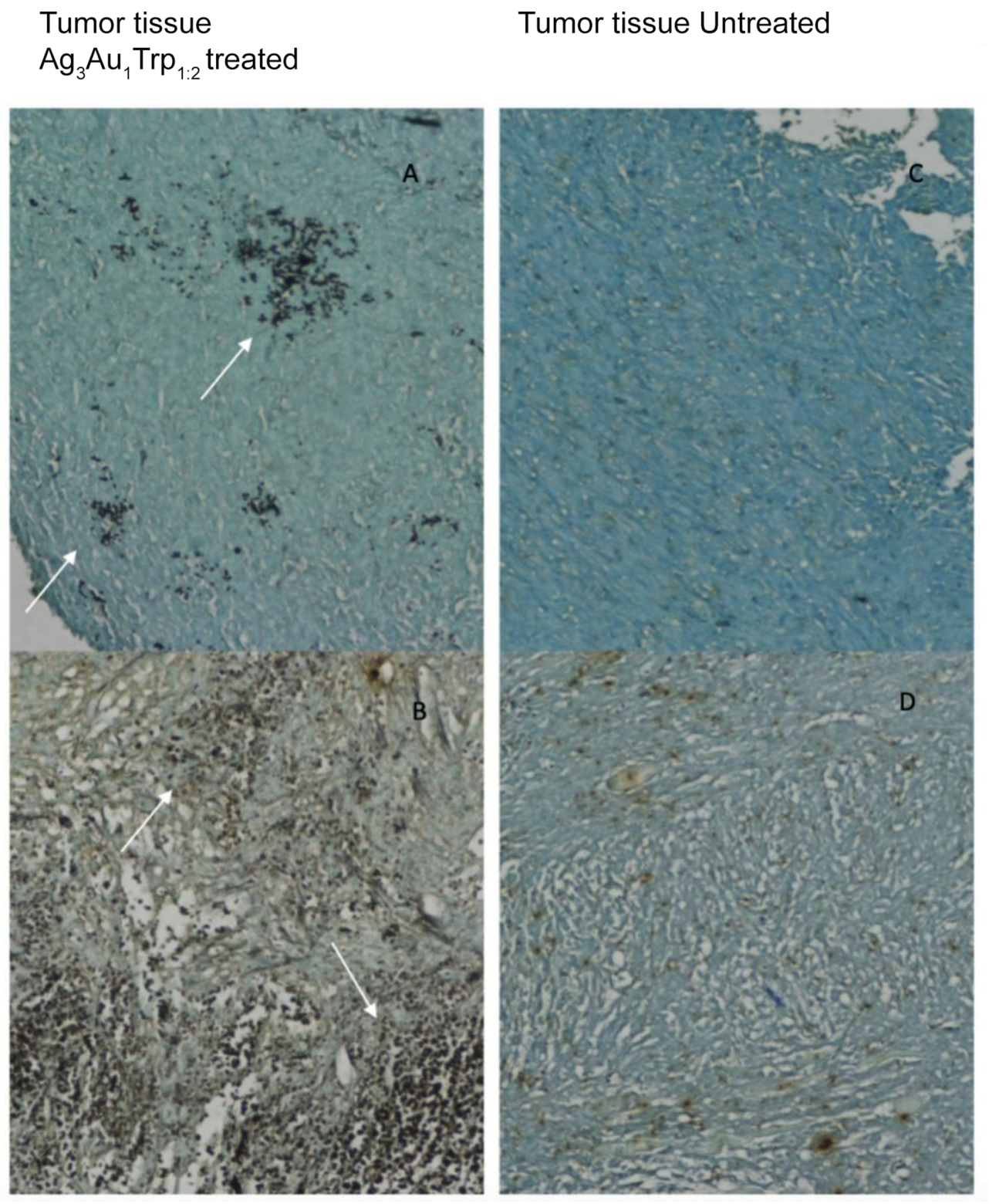

Figure 7 Arrows show $Ag_3Au_1Trp_{1:2}$NPs which are visible as black spots in tumor tissue from mice that received treatment (**A** and **B**). (**C** and **D**) show tumor tissue from untreated mice. Methylene blue was used as counterstain.

complex (DISC) and the recruitment of an adaptor molecule, Fas-associated protein with death domain (FADD), and subsequent binding and activation of caspase-8 and −10. Activated caspase-8 and −10 then cleave caspase-3, which in turn leads to cleavage of the death substrates.[24] Expression studies (Western blot analysis) demonstrated

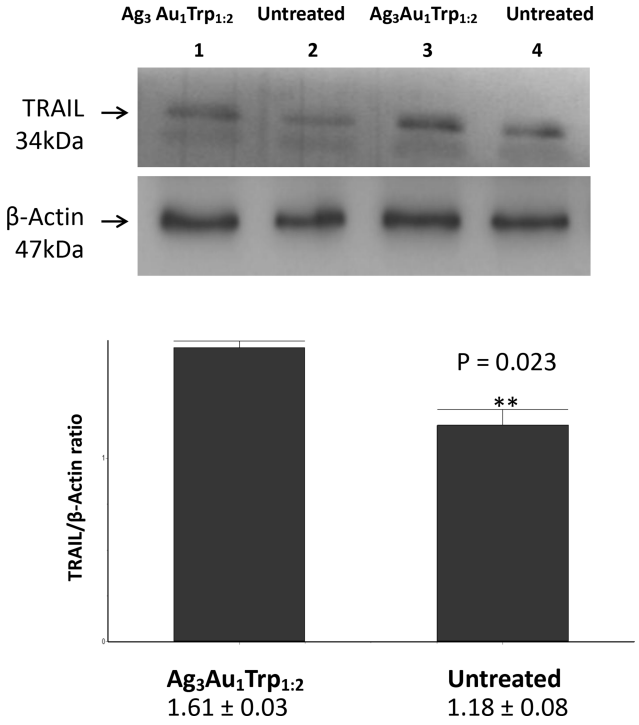

Figure 8 Fold change in the levels of TRAIL protein between cancer tissue of mice treated with $Ag_3Au_1Trp_{1:2}$NPs and untreated. The symbol **show statistical significance using one-way ANOVA ($p < 0.01$) compared to treated mice.

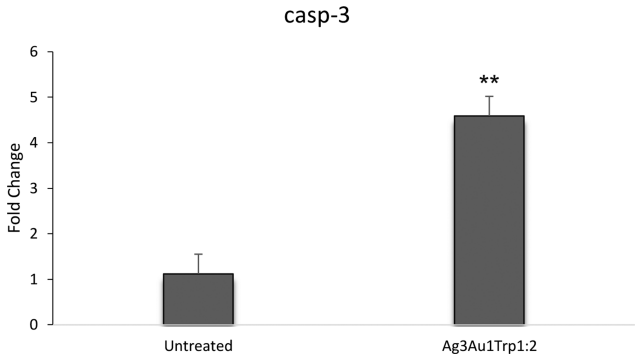

Figure 9 *Casp-3* fold change in tumors from mice that received $Ag_3Au_1Trp_{1:2}$NPs treatment. The symbol **show statistical significance using one-way ANOVA ($p < 0.01$) compared to untreated mice.

that TRAIL was over-expressed in SCID cancer tissue under the treatment with $Ag_3Au_1Trp_{1:2}$NPs, leading subsequently to the over-regulation (Real-time PCR) of Caspase-3.

Conclusion

$Ag_3Au_1Trp_{1:2}$NPs are an effective therapeutic tool that is proven to have anti-tumor effect in vivo. Additionally, a relatively high percentage of BNPs reaches the tumor via EPR effect, which selectively triggers apoptotic responses in cancer cells rather than in non-cancerous cells via the extrinsic TRAIL-dependent pathway. Furthermore, $Ag_3Au_1Trp_{1:2}$ NPs show anti-metastatic potency in vitro, since their presence inhibited wound closure; compared to untreated cells, cells incubated with $Ag_3Au_1Trp_{1:2}$NPs completed only a tenth of the closure process. The absence of metastatic sites in vitro in mice that received $Ag_3Au_1Trp_{1:2}$NPs highlights this anti-metastatic effect even more.

Acknowledgment

The authors gratefully acknowledge Mr. Stavros Xanthopoulos, INRASTES, NCSR "Demokritos", for excellent technical assistance.

Funding

This research is co-financed by Greece and the European Union (European Social Fund – ESF) through the Operational Programme Human Resources Development, Education and Lifelong Learning in the context of the project "Strengthening Human Resources Research Potential via Doctorate Research −2nd Cycle" (MIS-5000432), implemented by the State Scholarships Foundation (IKY).

Disclosure

The authors report no conflicts of interest in this work.

References

1. Parvanian S, Mostafavi SM, Aghashiri M. Multifunctional nanoparticle developments in cancer diagnosis and treatment. *Sens Biosensing Res*. 2013;13:81–87. doi:10.1016/j.sbsr.2016.08.002
2. Gazouli M, Lyberopoulou A, Pericleous P, et al. Development of a simple and sensitive quantum dot labelled magnetic immunoassay method for circulating colorectal cancer cell detection. *World J Gastroenterol*. 2012;18(32):4419–4426. doi:10.3748/wjg.v18.i32.4419
3. Katifelis H, Lyberopoulou A, Mukha I, et al. Ag/Au bimetallic nanoparticles induce apoptosis in human cancer cell lines via P53, CASPASE-3 and BAX/BCL-2 pathways. *Artif Cells Nanomed Biotechnol*. 2018;46(sup3):S389–S398. doi:10.1080/21691401.2018.1495645
4. Muthu MS, Mei L, Feng SS. Nanotheranostics: advanced nanomedicine for the integration of diagnosis and therapy. *Nanomedicine (Lond)*. 2014;9(9):1277–1280. doi:10.2217/nnm.14.83
5. Peng J, Liang X. Progress in research on gold nanoparticles in cancer management. *Medicine (Baltimore)*. 2019;98(18):e15311. doi:10.1097/MD.0000000000015311
6. Shmrakov I, Mukha I, Vityuk N, et al. Antitumor activity of alloy and core-shell-type bimetallic AgAu nanoparticles. *Nanoscale Res Lett*. 2017;12:333.
7. Yeh YC, Creran B, Rotello VM. Gold nanoparticles: preparation, properties and applications in bionanotechnology. *Nanoscale*. 2012;4(6):1871–1880. doi:10.1039/c1nr11188d

8. Lee SH, Jun BH. Silver nanoparticles: synthesis and application for nanomedicine. *Int J Mol Sci*. 2019;20(4):865. doi:10.3390/ijms20040865
9. Mukha I, Vityuk N, Galina G, et al. Anticancer effect of Ag, Au, and Ag/Au bimetallic nanoparticles prepared in the presence of tryptophan. *J Nanosci Nanotechnol*. 2017;17(12):8987–8994(8). doi:10.1166/jnn.2017.14106
10. Justus CR, Leffer NM, Echevarria MR, et al. In vitro cell migration and invasion assays. *J Vis Exp*. 2014;88:e51046.
11. Zhernosekov KP, Filosofov DV, Baumet RP, et al. Processing of generator-produced 68Ga for medical application. *J Nucl Med*. 2007;48(10):1741–1748. doi:10.2967/jnumed.107.040378
12. Yook S, Cai Z, Lu Y, et al. Intratumorally injected 177Lu-labeled gold nanoparticles: gold nanoseed brachytherapy with application for neoadjuvant treatment of locally advanced breast cancer. *J Nucl Med*. 2016;57:936–942. doi:10.2967/jnumed.115.168906
13. Wang Z, Jacobson O, Tian R. Radioligand therapy of prostate cancer with a long-lasting prostate-specific membrane antigen targeting agent 90Y-DOTA-EB-MCG. *Bioconjug Chem*. 2018;29:2309–2315. doi:10.1021/acs.bioconjchem.8b00292
14. Sabbagh L, Bourbonnière M, Sékaly RP, Cohen LY. Selective up-regulation of caspase-3 gene expression following TCR engagement. *Mol Immunol*. 2005;42:1345–1354. doi:10.1016/j.molimm.2004.12.011
15. Lin J, Zhang Z, Zeng S, et al. TRAIL-induced apoptosis proceeding from caspase-3-dependent and -independent pathways in distinct HeLa cells. Biochem. *Biophys Res Commun*. 2006;346:1136–1141. doi:10.1016/j.bbrc.2006.05.209
16. Longmire M, Choyke PL, Kobayashi H. Clearance properties of nano-sized particles and molecules as imaging agents: considerations and caveats. *Nanomedicine (Lond)*. 2008;3(5):703–717. doi:10.2217/17435889.3.5.703
17. Choi HS, Liu W, Misra P, et al. Renal clearance of nanoparticles. *Nat Biotechnol*. 2007;25(10):1165–1170. doi:10.1038/nbt1340
18. Tsoukalas C, Psimadas D, Kastis GA, et al. A novel metal-based imaging probe for targeted dual-modality SPECT/MR imaging of angiogenesis. *Front Chem*. 2018;6:Article 224. doi:10.3389/fchem.2018.00224
19. Chaves SB, Lavaca LM, Lavaca ZG, et al. Light microscopy and magnetic resonance characterization of a DMSA-coated magnetic fluid in mice. *IEEE Trans Magn*. 2002;38:3231–3233.
20. Monge-Fuentes V, Garcia MP, Henriques MC, et al. Biodistribution and biocompatibility of DMSA- stabilized maghemite magnetic nanoparticles in nonhuman primates. *Nanomedicine*. 2011;6:1529–1544. doi:10.2217/nnm.11.47
21. Hoshyar N, Gray S, Han H, et al. The effect of nanoparticle size on in vivo pharmacokinetics and cellular interaction. *Nanomedicine (Lond)*. 2016;11(6):673–692. doi:10.2217/nnm.16.5
22. Wilhelm S, Tavares AJ, Dai Q, et al. Analysis of nanoparticle delivery to tumours. *Nat Rev Mater*. 2016;1:16014. doi:10.1038/natrevmats.2016.14
23. Ashkenazi A. Targeting death and decoy receptors of the tumour-necrosis factor superfamily. *Nat Rev Cancer*. 2002;2(6):420–430. doi:10.1038/nrc821
24. Hunt A, Evan G. Apoptosis. Till death us do part. *Science*. 2001;293(5536):1784–1785. doi:10.1126/science.1065206